

Characterization of Nanostructured and Ultrafine-Grain Aluminum-Silicon Claddings using the Nanoindentation Technique

J. ARREGUIN-ZAVALA,¹ J. MILLIGAN,¹ M.I. DAVIES,² S.R. GOODES,²
and M. BROCHU^{1,3}

1.—Department of Mining and Materials Engineering, McGill University, Montreal, QC H3A 0C5, Canada. 2.—Micro Materials Limited, Willow House, Yale Business Village, Wrexham LL13 7YL, UK. 3.—e-mail: mathieu.brochu@mcgill.ca

The nanoindentation technique is an emerging characterization technique that permits measurement of dynamic properties on a small scale. This article reports results on the characterization of nanostructured and ultrafine-grained Al-Si claddings using this technique. First, it was found that with this technique, the dynamic hardness of the material also becomes independent of the load, similar to nanoindentation, which yields to the concept of the existence of a dynamic true hardness. Second, the plasticity results have been compared to a strain-gradient plasticity model and have shown to deviate from the Nix-Gao model. Finally, a comparison between H/E and DH/E ratios has shown that the DH/E ratio correlates better with dry sliding wear results obtained for this material.

INTRODUCTION

Aluminum (Al) alloys are used in several transportation applications in which the reduction of overall weight is targeted.¹ One of their main drawbacks is their poor wear resistance. To this end, in terms of monolithic alloys, the aluminum-silicon (Al-Si) alloys (either 4XXX or 3XX foundry alloys) are the best solution currently available.^{2,3} Their increased wear resistance, provided by the hard silicon (Si) phase, has been reported to increase with Si content up to the eutectic composition, after which conflicting data are reported.^{4–8} This discrepancy in the literature data comes as a result of the load variation in loading conditions. Increasing the load will lead to the fracture of primary Si particles resulting in crack initiation at the particle edges leading to more severe wear compared to an alloy with less Si content.⁹

Two general trends have been found in the literature to improve the sliding wear resistance of these alloys, namely (I) the refinement of the Si phase and (II) the increased circularity of the Si particles.^{7,10–13} The current authors have studied the fabrication of nanostructured and ultrafine-grained (UFG) Al-Si claddings on Al 7075 substrates processed by elec-

trospark deposition (ESD)¹⁴ and spark plasma sintering (SPS)¹⁵ of cryomilled Al-Si powders.¹⁶ Dry sliding wear testing of each cladding was undertaken, and it was observed that indeed, with increasing refinement of both the Al and Si phases, the wear resistance is increased.¹⁷ The wear rate of a material is often slowed by the formation of a mechanically mixed layer (MML), in which the continuous plastic deformation of the material transferred between the counterface and wear surface is occurring, resulting in a hardened layer at the surface.

One possible avenue to investigate deformation mechanisms of nanostructured or UFG materials to better understand wear is that of nanoindentation. Many researchers apply the Nix-Gao model, based on the Taylor dislocation model¹⁸ and a model of geometrically necessary dislocations (GNDs), to understand the plastic deformation of small-scale materials.¹⁹ The model, shown in Eq. 1, relates microindentation hardness H and the indentation depth h :¹⁹

$$\left(\frac{H}{H_0}\right)^2 = 1 + \frac{h^*}{h} \quad (1)$$

where h^* is a characteristic length that characterizes the depth dependence of the hardness and H_0 is

the hardness that would arise from the statistically stored dislocations alone, in the absence of any GNDs. A complete description of the GND formation during indentation can be found elsewhere.¹⁹ For low-strain-rate nanoindentation, it was reported that the hardness drops with the indentation load following the strain gradient plasticity model.²⁰ In such cases, the plasticity induced by the indentation would cause an increase in GNDs beneath the indenter. A major drawback of the nanoindentation approach is that deformation during wear, and in particular during dry sliding, occurs at a much higher strain rate than that realized during nanoindentation; therefore, the actual deformation mechanism during wear can be different to the one operating during nanoindentation.

The nanoimpact indentation technique represents an alternative to nanoindentation to investigate the plastic deformation under high-strain-rate conditions, and hence possibly provide more accurate information to better correlate with high-strain-rate wear processes. The quantification of instantaneous resistance to impact deformation is termed impact hardness (H_{imp}) or dynamic hardness (DH), and it is defined as the energy absorbed by the material during the impact and normalized by the plastically deformed volume.²¹ DH is calculated using Eq. 2:

$$DH = \frac{\text{Energy of impact}}{\text{Volume of indentation}} \approx \frac{(1/2)m(v_{in}^2 - v_{out}^2)}{(8.2)h^3} \quad (2)$$

where v_{in} and v_{out} are the velocity of the indenter as the pendulum swings into and out of the sample surface, m is the effective mass of the pendulum, and h is the penetration depth corresponding to the displaced volume specific to the indenter used. The DH is inferred from the difference in kinetic energies of the pendulum and penetration depth.²¹ This technique may employ an indenter with a conical or a trigonal pyramid (Berkovich geometry). This technique differs from traditional dynamic testing setup with respect to the contact volume, which is significantly smaller and, hence, can be focused on small areas.

The utilization of nanoimpact testing is emerging, but still significant work must be done to better understand the deformation mechanism under the indenter and how the results could be interpreted to provide useful scientific information on material behavior. In that respect, this article seeks to gain a better understanding of the technique when applied to metallic materials. This paper investigates (I) if the deformation during nanoimpact follows the strain gradient plasticity model during slow strain rate indentation and (II) if the use of a ratio dynamic hardness/Young modulus (DH/E) could better correlate with dry sliding wear response of materials. The experiments were carried out on nanostructured and UFG Al-12Si alloys, processed by SPS of cryomilled powders, and ESD.

EXPERIMENTAL PROCEDURES

The Al-12Si UFG claddings on 7075 were fabricated using cryomilled powder¹⁶ sintered using a Thermal Technology LLC 10-3 SPS press (Thermal Technology LLC, Santa Rosa, CA) in an ISO-Carb85 graphite die. The temperature was ramped at constant rate of 100°C/min to temperatures 350°C, 450°C, and 500°C and held for 120 s. A mechanical vacuum environment was maintained at 6.0×10^{-2} Torr prior to and throughout sintering. Temperature was measured using a C-type thermocouple set in a hole in the bottom punch drilled to 2 mm from the surface of the sample. A preload pressure of 15 MPa was applied prior to the temperature ramp and then increased to 50 MPa during heating and maintained while sintering.

The nanostructured Al-12Si claddings were fabricated by ESD using TechnoCoat MicroDepo Model 150 ESD machine (TechnoCoat, Shizuoka-Ken, Japan) in an argon atmosphere to prevent oxidation of the deposited material. A complete description of the deposition parameters and characterization of the microstructures can be found in Ref. 14.

The densities of the sintered compacts were measured by the Archimedes method according to ASTM Standard B962-08. Cross sections of the SPS pucks were mounted in bakelite, ground, and polished using, 240-, 400-, 600-, 800-, and 1200-grit SiC paper, followed by polishing with 3, 1- μ m diamond suspension and 0.05- μ m colloidal silica suspension. The Al grain size and Si particle size and distributions were determined by image analysis using Hitachi 4700SN and Hitachi SU-8000 Electron Microscope micrographs (Hitachi, Tokyo, Japan).

DH experiments were performed using the NanoTest Vantage impact module (MicroMaterials, Wrexham, U.K.) and a schematic of the pendulum fixture is shown in Fig. 1. The NanoTest loading

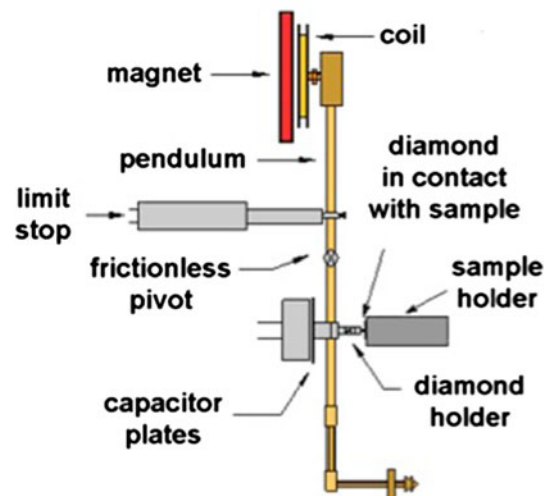


Fig. 1. Schematic of the nanoimpact pendulum setup.

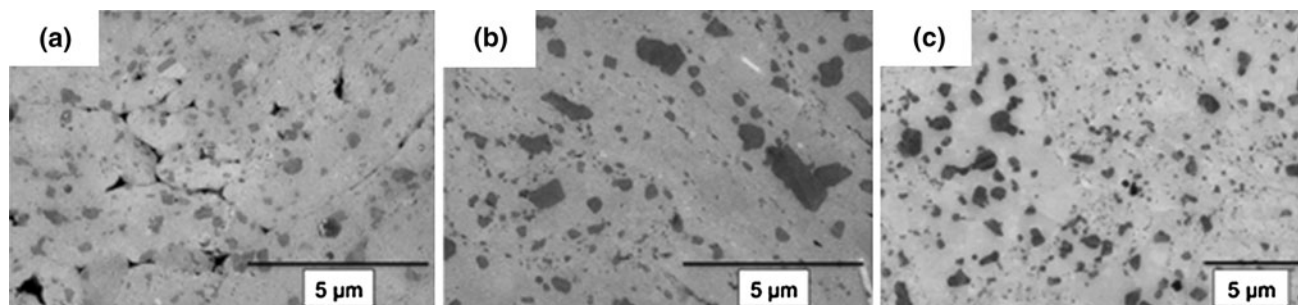


Fig. 2. SEM micrographs of the compacts sintered at (a) 350°C, (b) 450°C, and (c) 500°C.

Table I. Measured densities and average grain size for the Al and Si upon SPS

Temperature (°C)	Density (g/cm ³)	% of Theoretical Density	Al Grain Size (nm)	Si Particle Size (nm)
350	2.52	95	550 ± 340	240 ± 160
450	2.57	97	950 ± 520	340 ± 270
500	2.62	99	1100 ± 750	370 ± 260

head is based on a pendulum design. In impact experiments, a solenoid at the base of the pendulum is used to remove the indenter from the sample surface. This solenoid is then switched off, allowing the indenter to accelerate back to the sample surface. Variables such as the accelerating force can be set to allow contact at strain rates much higher than in conventional nanoindentation experiments. On impact penetration, the depth versus time data are collected. These data are then analyzed to determine the DH. A complete description of the analysis method can be found elsewhere.²¹ DH measurements were made at accelerating forces of 5 mN, 10 mN, 20 mN, 30 mN, and 40 mN, and ten experiments were performed at each force to obtain a statistically significant result. A conical indenter of semiapex angle equal to 71° was used to assess the validity of the GNDs model for nanoimpact and a cube corner indenter was used for the work related to the DH/E ratio.

RESULTS AND DISCUSSION

Comparison of the Nanoimpact Indentation Deformation with the Nix-Gao Model

This series of experiments was carried out on the UFG claddings, and prior to the presentation of the nanoimpact results, a brief summary of the characterization of the samples is presented.

Figure 2 presents secondary electron SEM micrographs of the claddings for the three sintering conditions. As expected, the microstructure is a two-phase structure with the Si particles well dispersed throughout the matrix. Table I presents the density measurements, Al grain size, and Si particle size upon the three tested sintering cycles. The density of each sample was compared to the theoretical

density (TD; 2.65 g/cm³) calculated from the rule of mixtures. The density after sintering at 350°C was found to be 95% TD, and further increased up to 99% with increasing temperature. Significant growth of both Al and Si phases occurs during the sintering process, and the final grain sizes are in the UFG and submicron range. The Al phase increases in average size from 550 ± 340 nm at 350°C to 1.1 ± 0.75 μm after sintering at 500°C. The Si phase size grows slower than the Al phase and reaches a final average size of 240 ± 160 nm after sintering at 350°C, 340 ± 270 nm after sintering at 450°C, and 370 ± 260 nm after sintering at 500°C. After sintering at 350°C, the Si particles had an average circularity of 0.84 ± 0.15, where a circularity of 1.00 represents a perfect circle. Increasing the temperature results in a statistically similar average circularity of 0.73 ± 0.15 and 0.73 ± 0.19 for sintering at 450°C and 500°C, despite the presence of Si agglomerations and particle impingement during the growth of the Si.

To investigate if the nanoimpact indentation agrees with the Nix-Gao model,¹⁹ the DH was measured as a function of the residual depth for the three sintered conditions and the results are presented in Fig. 3. As observed, the results obtained all display a decrease in the DH with an increasing indentation depth, and this behavior is independent of the sintering condition. It is also interesting to note that all the curves tend toward a plateau, for which the DH seems to become independent of the indentation depth. According to the Nix-Gao model,¹⁹ this plateau, denoted as H_0 in Eq. 1 for low-strain-rate indentation, is known as the true hardness of the material, a condition where only the stored dislocations influence the hardness.²⁰ By association, our results indicate the existence of a

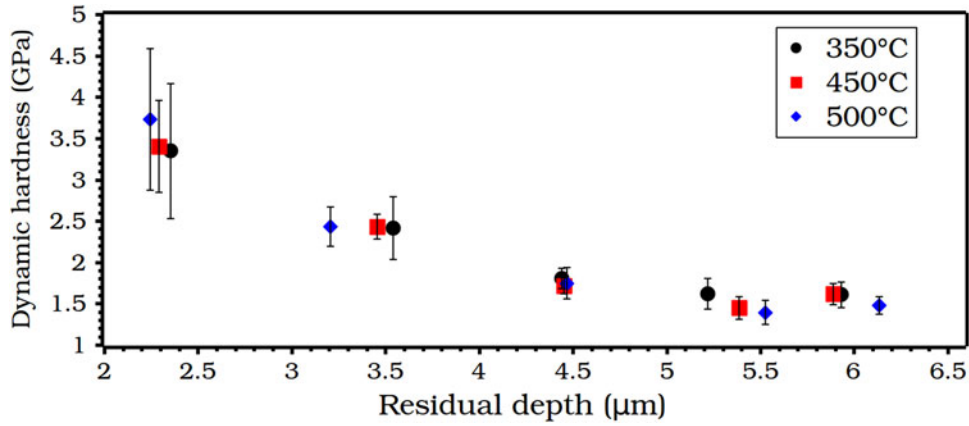


Fig. 3. DH as a function of residual indentation depth for claddings sintered at 350°C, 450°C, and 500°C.

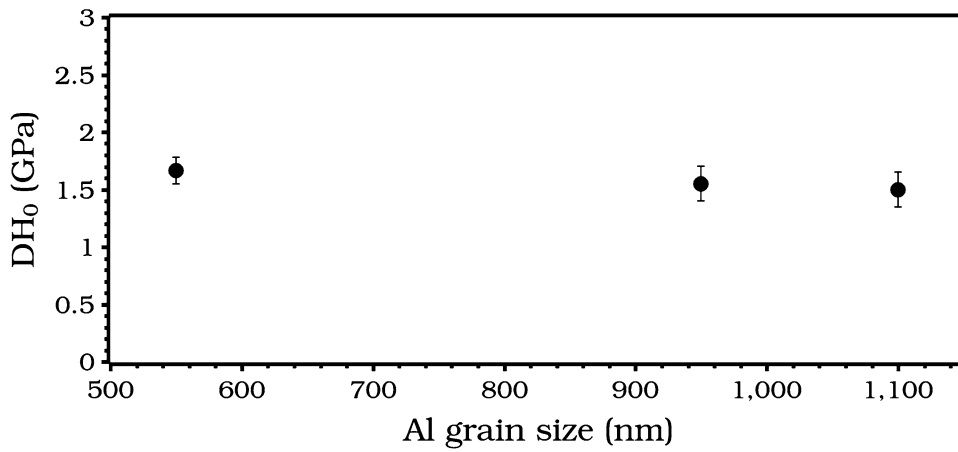


Fig. 4. Dynamic true hardness as a function of Al grain size.

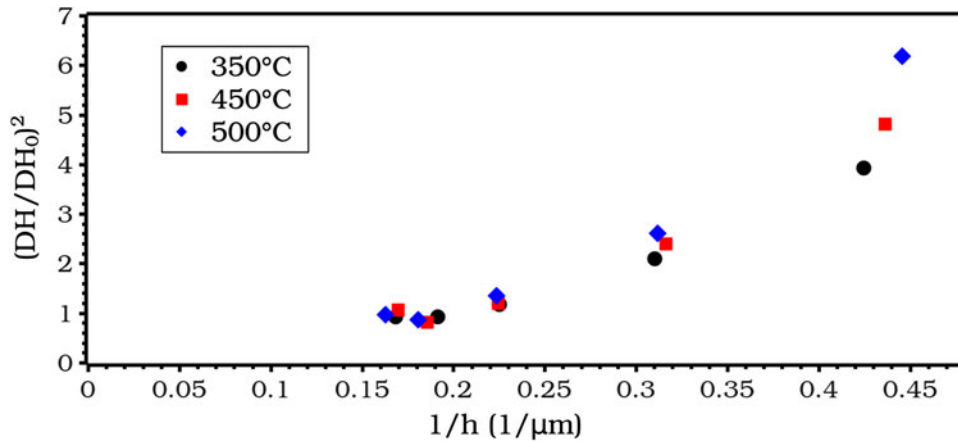


Fig. 5. Depth dependence of the DH for the UFG Al-Si claddings.

true DH (DH_0). The measured DH_0 for the three sintered conditions are plotted as a function of the Al grain size in Fig. 4 and depict that the DH_0 is statistically similar (~ 1.57 GPa). This infers that for the three tested grain sizes, the plasticity and

work-hardening behavior under the tested strain rate should be similar.

To investigate whether the Al-Si claddings behave according to the strain plasticity gradient model, the experimental results were plotted as $(DH/DH_0)^2$

Table II. Comparison between H/E and DH/E for two types of Al-12Si claddings

Method of Deposition of Al-Si Clad	H/E Calculated from Nanoindentation	Dynamic H/E from Nanoindentation
SPS	0.015	0.024
ESD	0.017	0.034

versus the inverse of the indentation depth, and the trend is presented in Fig. 5. To be in agreement with the Nix-Gao model,¹⁹ the results should lie on a straight line, intercepting the Y axis at 1. The current experimental results clearly indicate that the strain gradient plasticity model is not respected under high-strain-rate deformation. Previous researchers have modeled and experimentally investigated the dislocation formation under higher strain rates and have found that under high strain rates, the dislocation production is lower than at lower strain rate.^{22–24} The dislocation density increases slower with strain at high strain rates than at lower strain rates.^{22–24} This difference in the generation and densities of dislocations is believed to explain the deviation from the Nix-Gao model during nanoindentation. Further work is required in this area to develop a model explaining the nanoindentation trend observed. It is worth mentioning that results from McElhaney et al.²⁵ obey the plasticity model at corresponding indentations depth for cold-rolled Cu, strengthening our belief that the strain rate (i.e., dislocation activity) is the key explanation for the deviation observed in our results.

H/E Ratio Versus DH/E Ratio

Many researchers are looking at the plasticity index, which includes the ratio of the hardness (H) over the modulus of elasticity (E) of the material (H/E ratio), as it was found to correlate with the wear-resistance behavior; increasing the H/E ratio was found beneficial against sliding and abrasion.^{13,26–28} However, in the case of dry sliding wear for example, because the strain rate is higher than what is typically found during nanoindentation, a possibly more appropriate analysis would be to consider a dynamic H/E ratio (DH/E), which should yield a more realistic correlation with the wear resistance. In this case, for the UFG cladding possessing a Young modulus of 87.9 ± 3.7 GPa (E was measured by nanoindentation) and the obtained values of DH_0 (see Fig. 4), a DH/E ratio of 0.019, 0.018, and 0.017, was calculated for the three sintering conditions. These results show that the three microstructures should behave in a similar manner with respect to the plastic deformation occurring during wear. Consequently, because the claddings are produced by SPS (powder-base approach), the strength of the prior particle boundary becomes the key feature for wear resistance and not the microstructure itself.

To provide an additional insight on this concept, a comparison of the H/E (obtained from nanoindentation technique) and DH/E (obtained from nanoindentation technique) is presented in Table II. It is worth mentioning that for the comparison of the DH/E , the measurements for the SPS and ESD samples (complete microstructure characterization of ESD is found in Ref. 14) were made at 5 mN because larger loads would yield too large an indentation for the thin ESD cladding. The results show that using the nanoindentation technique (slow strain rate), the H/E is similar for the two types of claddings. However, a large difference was obtained for the DH/E (high strain rate) between the two samples, where a higher ratio is found for the ESD. This result correlates well with the dry sliding experiments performed on the two claddings, where the wear loss volume was one order of magnitude lower for the ESD samples than for the SPS cladding.¹⁷ This modified analysis would require additional experimental validation but is a possibly interesting avenue to further characterize and correlate with higher strain rate wear processes.

SUMMARY

This article has presented results on nanoindentation to characterize nanostructured and UFG Al-Si claddings processed by SPS and ESD. Particularly, this technique has shown that for the range of tested sintering temperatures, the claddings all have a similar dynamic true hardness. The results have also confirmed that the model of plastic deformation proposed by Nix-Gao is not valid for nanoindentation. Finally, an analysis of a newly proposed DH/E ratio provides a better correlation than the H/E ratio with the dry sliding wear results previously published.

REFERENCES

1. M. Bidmon, H. Valadon, R. Ebner, and J. Loeffler, *Nano-material Roadmap 2015; 6th Framework Program. SWOT Analysis Concerning the Use of Nanomaterials in the Automotive Sector*, 2005, pp. 1–14.
2. A.H. Committee, *ASM Handbook, 18, Friction, Lubrication and Wear Technology* (Materials Park, OH: ASM International, 1992).
3. E.P. Becker, *Tribol. Int.* 37, 569 (2004).
4. J. Clarke and A.D. Sarkar, *Wear* 54, 7 (1979).
5. D.K. Dwivedi, *J. Mater. Des.* 31, 2517 (2010).
6. K.M. Jasim and E.S. Dwarakadasa, *Wear* 119, 119 (1987).
7. M. Elmadagli, T. Perry, and A.T. Alpas, *Wear* 262, 79 (2007).

8. A.D. Sarkar and J. Clarke, *Wear* 75, 71 (1982).
9. M.A. Martinez, A. Martin, and J. Llorca, *Scr. Metall. Mater.* 28, 207 (1993).
10. A. Bendijk, R. Delhez, L. Katgerman, Th.H. Keijser, E.J. Mittemeijer, and N.M. Van Der Pers, *J. Mater. Sci.* 15, 2803 (1980).
11. S. Hegde and K. Prabhu, *J. Mater. Sci.* 43, 3009 (2008).
12. A.S. Reddy, B.N.P. Bai, K.S.S. Murthy, and S.K. Biswas, *Wear* 171, 115 (1994).
13. A. Leyland and A. Matthews, *Wear* 246, 1 (2000).
14. J. Milligan, D.W. Heard, and M. Brochu, *Appl. Surf. Sci.* 256, 4009 (2010).
15. J. Milligan, R. Gauvin, and M. Brochu, *Philos. Mag.* 2013. doi:[10.1080/14786435.2013.777816](https://doi.org/10.1080/14786435.2013.777816).
16. J. Milligan, R. Vintila, and M. Brochu, *Mater. Sci. Eng. A* 508, 43 (2009).
17. J. Milligan, J.M. Shockley, R.R. Chromik, and M. Brochu, *Tribol. Int.* 2013 (submitted).
18. G.I. Taylor, *Proc. R. Soc. Lond. A* 145, 362 (1934).
19. W. Nix and H. Gao, *J. Mech. Phys. Solids* 46, 411 (1998).
20. D. Goldbaum, J. Ajaja, R.R. Chromik, W. Wong, S. Yue, E. Irissou, and J.-G. Legaux, *Mater. Sci. Eng. A* 530, 253 (2011).
21. G. Constantinides, C.A. Tweedie, N. Savva, J.F. Smith, and K.J. Van Vliet, *Exp. Mech.* 49, 511 (2009).
22. Z.Q. Wang, I.J. Beyerlein, and R. Lesar, *Philos. Mag.* 87, 2263 (2007).
23. P.S. Follansbee and U.F. Kocks, *Acta Metall.* 36, 81 (1988).
24. S.R. Chen and G.T. Gray III, *Metall. Mater. Trans. A* 27A, 2994 (1996).
25. K.W. McElhaney, J.J. Vlassak, and W.D. Nix, *J. Mater. Res.* 13, 1300 (1998).
26. A. Leyland and A. Matthews, *Surf. Coat. Technol.* 177–178, 317 (2004).
27. G.S. Fox-Rabinovich, S.C. Veldhuis, V.N. Scvorstov, and L.S. Dosbaeva, *Thin Solid Films* 469–470, 505 (2004).
28. B.D. Beake, G.S. Fox-Rabinovich, S.C. Veldhuis, and S.R. Goodes, *Surf. Coat. Technol.* 203, 1919 (2009).